

# Autonomous Nucleus Tracking for Comet/Asteroid Encounters: The STARDUST Example

Shyam Bhaskaran  
(818)354-3152  
shyam@nova.jpl.nasa.gov  
Joseph E. Riedel  
(818) 354-8724  
jer@radtran.jpl.nasa.gov  
Stephen L. Synnott  
(818)354-6933  
stephen.synnott@jpl.nasa.gov

Jet Propulsion Laboratory  
California Institute of Technology  
AIS 301-150  
4800 Oak Grove Drive  
Pasadena, California, 91101

*Abstract* STARDUST is a mission to flyby the comet Wild-2 in early 2004 and return samples of the coma to Earth. During its 120-150 km flyby of the comet nucleus, a secondary science goal is to obtain images of the nucleus using the onboard navigation camera. Due to the 40 minute round-trip light time, ground processing of navigation data to update pointing information to maintain the nucleus in the camera field-of-view is impractical. ‘J’bus, a simple, reliable, and fast algorithm was developed to close the navigation loop onboard during encounter. The algorithm uses images of the nucleus during approach to update target relative state information. This involves centroiding on the image to obtain nucleus center-of-figure data and then processing the data through a Kalman filter to update the spacecraft position and attitude. Monte Carlo simulations were then performed to test the algorithm. These simulations incorporated errors in spacecraft initial position and in attitude knowledge to provide a “truth” model which the filter must recover from. The results of the simulations proved that the algorithm was successful in maintaining the nucleus in the camera field-of-view assuming nominal values for the error sources. Even with worst case errors, the algorithm performed successfully in over 90% of the cases.

4. IMAGING SYSTEM
5. KALMAN FILTER SETUP
6. MONTE CARLO SIMULATION AND RESULTS
7. TIMING
8. CONCLUSIONS

## 1 INTRODUCTION

STARDUST, the fourth mission in NASA’s Discovery program, is a mission to be launched in early 1999, perform a relatively low velocity flyby of the comet P/Wild-2 in January, 2004, and return to Earth in 2006. Its primary science goal is to collect 1000 particles of cometary dust of greater than 15 microns during the flyby and return them to Earth in a sample return capsule. As secondary science goals, the spacecraft will also collect interstellar dust particles and obtain Wild-2 coma and nucleus images during the encounter. Due to the size of the navigation uncertainties at the time of the final uplink of the encounter sequence to the spacecraft, the tracking of the nucleus during the encounter using the onboard camera cannot be performed open-loop. In addition, the large (~40 minute round-trip light-time) precludes ground intervention during the encounter time period to update navigation information. Instead, images taken with the camera starting around 20 minutes prior to closest approach will be used to refine the co-incident spacecraft state, and therefore the camera boresight pointing direction to the comet, onboard the spacecraft itself. Because

## TABLE OF CONTENTS

1. INTRODUCTION
2. THE MISSION
3. NAVIGATION

of the tight turnaround needed to maintain lock, the on board algorithm has to be simple, reliable, and fast. It performs centroiding to determine the center of the comet nucleus, and incorporates this information into Kalman filter to update state information. This paper describes in detail the algorithms used, and the results of simulations to verify the code.

## 2 THE MISSION

STARDUST is the fourth mission of NASA's Discovery program, following Mars Pathfinder, Near Earth Asteroid Rendezvous, and Lunar Prospector. The mission is a collaborative effort, with JPL providing the project management, navigation, and mission design capabilities, Lockheed Martin Astronautics in Denver, CO providing the spacecraft and most mission operations, and the University of Washington, where the Principal Investigator is located. The spacecraft will be launched in mid-February, 1999 aboard a Delta 7436 launch vehicle. During its 5 year cruise to the comet P/Wild-2, it will perform one gravity assist using the Earth to give it enough energy to rendezvous with the comet. Comet flyby will occur on January 1, 2004 at a comet-relative velocity of a little over 6 km/s. During this flyby, a unique substance known as aerogel, developed at the Jet Propulsion Laboratory, will be deployed to collect coma dust particles. The vehicle itself will be protected from the hypervelocity impacts of these particles using a forward facing shield (termed the "Whipple" shield, in honor of astronomer Fred Whipple). The primary science requirement is to collect at least 1000 particles of greater than 15 micron size which embed themselves in the aerogel as the spacecraft flies by the comet. Due to the uncertainty in the models which describe the density of dust surrounding the nucleus, the actual flyby distance is still somewhat uncertain, and involves a trade-off between spacecraft safety and meeting the 1000 particle requirement. With current coma models, the distance is set between 120 and 150 km, but the uncertainty in the models is roughly a factor of 2 or 3. Also during the flyby, coma and nucleus images will be taken by the onboard camera through color filters and downlinked in real-time to the ground, except for a  $\pm 4$  minute period surrounding encounter when the images will be stored for later playback.

To maintain the comet in the camera field-of-view (FOV) during approach, encounter, and departure, the boresight of the camera must sweep through nearly 180° in angle. Rather than mount the camera on a scan platform (an expensive solution both in cost, complexity, and mass), this task is accomplished by means of a mirror which is free to rotate about one axis such that it rotates in the orbital plane of the flyby. At 180 seconds prior to encounter, the spacecraft performs a roll maneuver to place the comet in the mirror plane of rotation. In addition, to see the

comet during approach when it is hidden from view by the Whipple shield, a periscope is mounted which peers around the shield. This camera/mirror/periscope combination forms the imaging system which doubles as both the science and optical navigation instrument.

After collecting the samples, the aerogel is stowed into a sample return capsule equipped with an aeroshell where it will remain for the rest of the mission. The spacecraft then retargets its trajectory for an Earth return to occur 011 January 13, 2006. At E-1 days, the spacecraft performs its final maneuver to target the SRC for a landing within a 60 by 6.5 km footprint at the Air Force's Utah Test and Training Range (UTTR) facility. Several hours prior to entry, the SRC is jettisoned from the main spacecraft bus, which then performs a divert maneuver to keep it from also entering the Earth's atmosphere. After landing at UTTR, the aerogel with the samples is recovered from the SRC and sent to a facility at the Johnson Space Center for storage and dissemination to the science team. For more information on the STARDUST mission, see its homepage 011 the World Wide Web at <http://stardust.jpl.nasa.gov/>.

## 3 NAVIGATION

The primary mode of navigation for the mission will be standard X-band Doppler and ranging. Covariance analysis has shown that this is sufficient to meet the requirements for all deep-space maneuvers, Earth gravity assist, and Earth return. For comet flyby however, the a-priori uncertainties in the comet ephemeris (around 1500 km) from ground-based observations preclude using radio data alone to navigate this phase of the mission. Therefore, the onboard camera must be used to take images of the comet prior to encounter to improve the comet ephemeris knowledge sufficient to meet the 120-150 km flyby requirement. Starting at Wild-2 encounter (W)-100 days, images will be taken at the rate of once per week. These will increase in frequency to twice per week at W-50 days, once per day at W-7 days, and once per hour at W-1 day. These optical navigation (OPNAV) images are used to support four Trajectory Correction Maneuvers (TCMs), occurring at W-30 days, W-10 days, W-2 days, and M-6 hours. Concurrent science images taken at the same frequency are also used to refine the coma model to determine dust density. A final decision on the actual flyby distance will be made and implemented at the W-2 day TCM. With the combination of radio and OPNAV data, the delivery of the spacecraft to its aimpoint at the final Wild-2 targeting TCM will be accurate to roughly 8 km in the cross-track direction, and 150 km (or 24 seconds) in the down-track, or time-to-go, direction, (all  $1\sigma$ ).

These delivery accuracies are sufficient to maintain spacecraft safety and meet the primary science requirement

assuming the minimum encounter distance does not go below 120 km. However, they are not sufficient to support the secondary goal of encounter nucleus imaging. In particular, the cross-track uncertainty is not small enough to determine the exact orbital plane to which the spacecraft must roll. Also, the down-track uncertainty is too large to determine which direction to point the mirror in the minutes surrounding closest approach. OPNAV images taken past the final targeting TCM will, of course, provide very accurate information which can reduce both uncertainties, but the 40 minute round-trip light-time effectively rules out controlling the roll angle and mirror pointing angle from the ground. This is what necessitates using closed-loop onboard navigation to maintain visual lock on the nucleus by the camera to meet the imaging science requirements. The procedure during encounter will be to initialize the onboard navigator with comet-relative position and velocity information obtained from standard ground navigation at 20 minutes prior to the nominal encounter time. From this time onward, images will be taken at 10 second intervals and processed by the onboard navigator to update the spacecraft position. This provides a new line-of-sight (LOS) pointing vector to the comet which is passed back to the spacecraft Attitude Control System (ACS). The pointing vector information is then combined with current spacecraft attitude knowledge by the ACS to determine the correct mirror angle for the next image. In addition, the updated spacecraft ephemeris also provides information on the flyby orbital plane; ACS will compute the roll angle needed to place the camera/mirror in this plane and execute the turn at the proper time. The entire process requires a tight loop between the onboard navigator and the ACS. The remainder of the paper will now describe in detail the algorithms and tests used to verify the navigation portion of the autonomous nucleus tracking system.

#### 4 IMAGING SYSTEM

There are three primary components to the imaging system used on STARDUST: the camera, mirror, and periscope. The camera is mounted such that the boresight points straight down the spacecraft  $-Y$  axis (see Figure 1). The mirror is then canted at a  $45^\circ$  angle to the camera boresight and allowed to swivel around the spacecraft  $Y$  axis such that the effective camera boresight viewing direction sweeps from the spacecraft  $+X$  axis to the  $-Z$  axis and finally to the  $-X$  axis with the convention that  $0^\circ$  mirror angle is  $+X$ ,  $90^\circ$  is  $-Z$ , and  $180^\circ$  is  $-X$ . During encounter, the spacecraft will be oriented such that the spacecraft  $+X$  axis (where the Whipple shield is located) is along the comet-centered spacecraft velocity vector, and the spacecraft  $X-Z$  plane is coincident with the comet-centered orbital plane of the flyby. If the navigation delivery were perfect then, the comet would be located at exactly  $-Z$  at encounter. The periscope is a

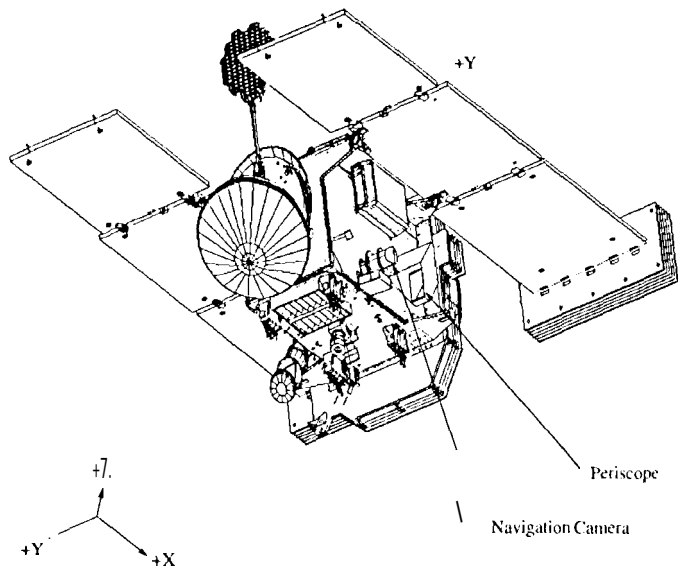


Figure 1: Spacecraft Configuration

two mirror system and is used to look at the approaching comet around the Whipple shield, but (assuming no misalignments) does not change the boresight viewing direction of the camera.

The camera itself has a 200 mm focal length lens which focuses light onto a  $1024 \times 1024$  Charge Coupled-Device (CCD) array. The angular FOV of the camera is  $3.5^\circ$ . For science purposes, the comet will be imaged through seven color filters mounted on a filter wheel. A clear filter for maximum light transmission is also provided for navigation images. To control the amount of light exposed to the CCD, the camera is equipped with a shutter which has a minimum shutter speed of 5 ms and a maximum of infinity. Analysis has shown that at encounter, the minimum speed should be fast enough to keep the comet from being overexposed.

#### 5 KALMAN FILTER SETUP

##### Introduction

The purpose of the Kalman filter is to use the onboard data to correct the nominal comet relative spacecraft position so that the camera will be pointed in the right direction to capture the nucleus in future images. The nominal comet relative spacecraft ephemeris is provided by ground-based navigation. The sole datatype used by the onboard navigator for nucleus tracking is the image of the comet. By determining the center of the nucleus in the image, the LOS direction of the comet from the spacecraft can be computed. Explicitly though, the LOS to the nucleus is not actually computed from the image; instead, the pixel and line (the  $x$  and  $y$  coordinates in the CCD image) location of the nucleus center is determined

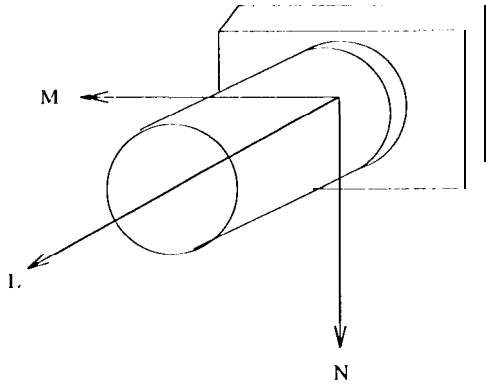


Figure 2: Camera Frame

from the image and differenced with predicts of the center location to obtain data residuals. These residuals are then processed by the Kalman filter to get corrections to the a-priori state.

### Observable Generation

In order to compute predicts of the comet location in the camera FOV, the transformation of an inertial vector into camera pixel and line coordinates is needed. This is a three step process; the first step is to rotate an inertial vector into a camera coordinate frame (the  $M$ - $N$ - $L$  frame shown in Figure 2), the second is to project these 3-D coordinates into the 2-D camera focal plane, and then finally scale the result into values of pixel and line. In the following derivation, the notation  $R_1(\theta)$ ,  $R_2(\theta)$ , and  $R_3(\theta)$  will be used to denote positive  $\theta$  rotations about the  $x$ ,  $y$ , and  $z$  axes, respectively.

First, we need the inertial to spacecraft body-fixed rotation matrix,  $T_{IBF}$ . This is provided by the ACS system using information from the star tracker or gyroscopes. The rotation to the camera  $M$ - $N$ - $L$  coordinate system requires several steps. Recall that the camera boresight,  $L$ , is pointed in the spacecraft  $-Y'$  axis, which puts the camera  $M$ - $N$  plane in the spacecraft  $X$ - $Z$  plane. The orientation of  $M$ - $N$  is defined with  $M$  parallel to  $X$  and  $N$  parallel to  $Z$ . If the mirror angle,  $\theta$ , is  $0^\circ$  (i.e., the mirror is pointed along the spacecraft  $X$  axis), the reflection effectively transforms  $M$ - $N$ - $L$  to  $M'$ - $N'$ - $L'$  such that  $L'$  is now along  $X$ ,  $M'$  points in  $-Y$ , and  $N'$  remains the same (Figure 3). This transformation can be accomplished via

$$T_1 = R_r R_3(90^\circ) R_2(90^\circ), \quad (1)$$

where

$$R_r = \begin{bmatrix} -1 & 0 & 0 \\ 0 & 1 & 0 \\ 0 & 0 & 1 \end{bmatrix}. \quad (2)$$

The matrix,  $R_r$ , accounts for the mirror reflection about the  $X$ - $Z$  plane which flips  $M$  from  $Y$  to  $-Y$ , with the re-

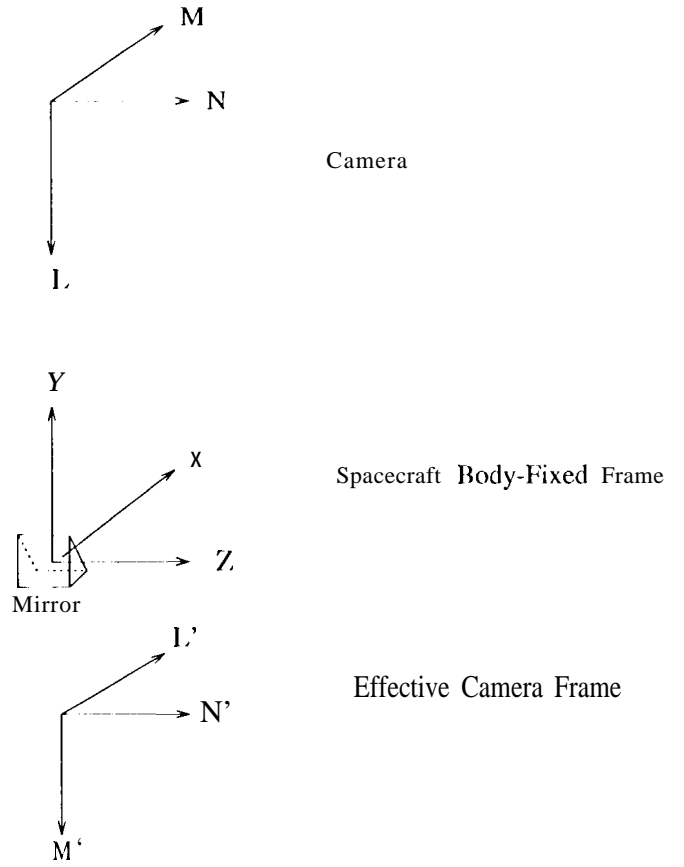


Figure 3: Spacecraft and Camera Coordinate Frames

suit that  $M'$ - $N'$ - $L'$  is no longer a right-handed coordinate system.

Now, as the mirror swivels about the  $Y$  axis with angle  $\theta$ ,  $L'$  will sweep through the  $X$ - $Z$  plane. In addition, since the camera is fixed while the mirror swivels, the image will appear to rotate about the boresight. This rotation is applied as,

$$T_2 = R_3(\theta) R_1(\theta), \quad (3)$$

where the second term is a positive rotation about  $-M'$  (since the coordinate system is not right-handed) to align the boresight, and the first term rotates around the boresight. The total transformation from inertial to the camera frame,  $T_{IC}$  is then

$$T_{IC} = T_2 T_1 T_{IBF}. \quad (4)$$

An inertial LOS vector,  $\vec{V}_I$ , can then be rotated into a vector in the camera coordinates,  $\vec{V}_C$  by

$$\vec{V}_c = \begin{bmatrix} V_{c1} \\ V_{c2} \\ V_{c3} \end{bmatrix} = T_{IC} \vec{V}_I. \quad (5)$$

For a different orientation of the camera mounting) the procedure followed would be the same except that  $\pm 90^\circ$  or  $\pm 180^\circ$  would need to be added to the  $R_3$  rotation

in Eq. (1), and a different reflection matrix would be needed.

Once  $\vec{V}_c$ , a LOS vector in camera  $M-N-L$  coordinates is obtained, it needs to be transformed into the 2-D camera focal plane. A detailed description of this process can be found in [1]; a brief synopsis will be given here. First, apply the gnomonic projection,

$$\begin{bmatrix} x \\ y \end{bmatrix} = \frac{f}{V_{c3}} \begin{bmatrix} V_{c1} \\ V_{c2} \end{bmatrix} \quad (6)$$

where

- $f$  = the camera focal length, in mm
- $V_{c1}, V_{c2}, V_{c3}$  = the components of the line-of-sight vector in  $M-N-L$  coordinates
- $x, y$  = the projection of the LOS vector into focal plane coordinates, measured in mm.

Next, find the bias to  $x$  and  $y$ ,  $\Delta x$  and  $\Delta y$ , caused by optical distortions by:

$$\begin{bmatrix} \Delta x \\ \Delta y \end{bmatrix} = Q \begin{bmatrix} \nu_1 \\ \nu_2 \\ \nu_3 \\ \nu_4 \\ \nu_5 \\ \nu_6 \end{bmatrix}, \quad (7)$$

with

$$Q = \begin{bmatrix} -yr & xr^2 & -yr^3 & xr^4 & xy & x^2 \\ xr & yr^2 & xr^3 & yr^4 & y^2 & xy \end{bmatrix} \quad (8)$$

where  $r = x^2 + y^2$ , and the  $\nu$ 's are the optical distortion coefficients. The corrected image locations,  $x'$  and  $y'$ , are then

$$\begin{bmatrix} x' \\ y' \end{bmatrix} = \begin{bmatrix} x + \Delta x \\ y + \Delta y \end{bmatrix}. \quad (9)$$

Finally, the conversion from the rectangular coordinates to pixel and line is:

$$\begin{bmatrix} p \\ l \end{bmatrix} = \begin{bmatrix} K_x & K_{xy} & K_{xxy} \\ K_{yx} & K_y & K_{yyx} \end{bmatrix} \begin{bmatrix} x' \\ y' \\ x'y' \end{bmatrix} + \begin{bmatrix} p_o \\ l_o \end{bmatrix}, \quad (10)$$

where  $K$  is a transformation matrix from mm to pixel/line space, and  $p_o$  and  $l_o$  are the center pixel and line of the CCD. Currently, the  $\nu$ 's in Eq. (7) and all cross terms in the  $K$  matrix in Eq. (10) are set to zero. During flight, calibration images of dense star fields will be taken and used to accurately determine these parameters.  $K_x$  and  $K_y$  for the STARDUST camera is 83.8 pixels/mm.

## Centerfinding

Centerfinding is the process of obtaining the center of the target object in the image for use by the filter. Historically, this process has been refined through the Voyager encounters with Neptune and Uranus such that accuracies of much less than a pixel are possible [2], [3]. The pictures taken by the spacecraft of planetary satellites were sent to the ground for processing. Here, an analyst would first determine a rough center by eye; computer algorithms which model the ellipsoidal shape of the target with correct lighting due to phase angles and albedo variations could then refine the center location guess to a high accuracy. For STARDUST however, the centroiding must be done onboard without human intervention on an object with unknown size, shape and albedo properties, and with the additional complexity of random bright arcs appearing due to comet outgassing.

Currently, the only closeup images of a comet from a spacecraft were taken by the Giotto spacecraft as it flew by Halley in 1986. The images show multiple, large bright jets emanating from the comet and a dark nucleus barely visible. To the human eye at least, it appears that a brightness centroiding algorithm would pick a location outside of the nucleus, which would require a much more complicated algorithm to locate the nucleus. Fortunately, Wild-2 should be considerably less active than Halley was with the result that, when the spacecraft is inside the coma, the nucleus should be the brightest object in the image. In addition, outgassing activity should also be less frequent over the encounter time span and over a smaller spatial extent around the nucleus.

For these reasons, it was decided to use a simple brightness moment algorithm as the first step in the centerfinding process,

$$p_{cb} = \frac{\sum_{j=1}^N \sum_{i=1}^N iP_{ij}}{\sum_{j=1}^N \sum_{i=1}^N P_{ij}}, \quad l_{cb} = \frac{\sum_{j=1}^N \sum_{i=1}^N jP_{ij}}{\sum_{j=1}^N \sum_{i=1}^N P_{ij}}, \quad (11)$$

where  $P_{ij}$  is the brightness value at pixel  $i$  and line  $j$ ,  $A$  is 1024, and  $p_{cb}$  and  $l_{cb}$  are the computed brightness centers. In addition, the  $P_{ij}$ s are chosen such that

$$P_{min} \leq P_{ij} \leq P_{max} \quad (12)$$

where  $P_{min}$  is the minimum background noise value and  $P_{max}$  is the limit beyond which the brightness probably represents unusual outgassing activity. The actual values for these boundaries will depend on calibrations done during flight and far encounter when comet models will be improved.

This algorithm produces a center-of-brightness estimate (COB); what is needed is the center-of-figure (COF). If

the object were spherical, a simple correction factor computed as a function of the solar phase would suffice to obtain the COB-COF offset and the resulting COF estimate would be accurate to the pixel level. Although it is highly unlikely that Wild-2's nucleus is spherical, the offset is still applied to remove gross errors in the COB to COF offset. The formula is

$$\gamma = \frac{3\pi R}{16} \left[ \frac{\sin \alpha (1 + \cos \alpha)}{7(\pi - \alpha) \cos \alpha + \sin \alpha} \right] \quad (13)$$

where the offset factor,  $\gamma$  can take values between 0 and 1 to represent the offset as a fraction of the assumed object radius,  $R$ .  $\alpha$  is the phase angle, which, during encounter, will vary between  $70^\circ$  during approach to  $10^\circ$  at encounter. To apply the correction then, first find the direction of the sun in the camera coordinates by rotating the inertial LOS vector to the sun,  $A$  using  $T_{IC}$  from above, i.e.,  $A_c = T_{IC} A$ . Then, compute the sun direction in the image,  $\phi$ , measured clockwise from  $0^\circ$  in the positive pixel direction, as

$$\phi = \tan^{-1}(A_{cy}/A_{cx}). \quad (14)$$

The observed nucleus center is then:

$$p_o = p_{cb} - \gamma R_c \cos \phi \quad (15)$$

$$l_o = l_{cb} - \gamma R_c \sin \phi. \quad (16)$$

where  $R_c$  is the size of the nucleus transformed into pixel units. Given the range to the nucleus,  $\rho$ , from the nominal ephemeris,  $R_c$  can be computed as

$$R_c = \frac{RK_x f}{\rho}. \quad (17)$$

Because the true size and shape of the nucleus is unknown, the accuracy of the COF estimate is difficult to establish. For use in the Kalman filter, the COF data was weighted fairly conservatively, as will be described below. Loose weighting of the data also mitigates the effects of systematic biases introduced by using brightness centroids.

To minimize the possibility that brightness centroiding was performed on empty space or random noise, the search area to perform the centroiding is narrowed down by boxing a region around the a-priori guess at the center location. The box size is set by projecting the position uncertainty ellipsoid into the camera plane, taking the largest dimension of the ellipse, and adding tile size of the nucleus (a  $2.5\sigma$  ellipse is used). In addition, the integrated brightness in the centroided region must be above a certain threshold for the image to be valid. The value of the threshold is still to be determined and will depend on the observed sensitivities of the camera from calibration images taken in flight.

Table 1:  $1\sigma$  Values for Gyro Error Model Parameters

|                        |  |
|------------------------|--|
| Initial Attitude Error | 0.1 deg.                               |
| Random Attitude Noise  | $1.9 \times 10^{-4}$ deg.              |
| Gyro Drift Rate        | 0.0033 deg/hour,                       |
| Gyro Random Walk       | $0.025 \text{ deg}/\sqrt{\text{hour}}$ |

### Dynamics Model

The time frame during which the onboard navigation processing will be active is about the 20 minutes surrounding closest approach. Because the flyby distance is fairly large ( $> 100$  km) and the mass of the comet is fairly small, the trajectory during this time is essentially linear (perturbations caused by impacts with comet dust particles is also negligible). Thus, the trajectory model used by tile filter can safely assumed to be a straight line,

$$\vec{X}_t = \vec{X}_{t_0} + \vec{X}_t(t - t_0) \quad (18)$$

$$\vec{X}_t = \vec{X}_{t_0}. \quad (19)$$

where  $\vec{X}$  is the position and  $\vec{X}$  is the velocity, expressed in the comet-centered, J2000 Earth Mean Equatorial inertial coordinate system. The initial conditions,  $\vec{X}_{t_0}$  and  $\vec{X}_{t_0}$  when onboard navigation is started are provided by the results from ground-based navigation. The uncertainties in these initial conditions is largely in the position (around 8 km in the cross-track directions, 150 km in down-track), whereas the velocity is well determined from Doppler data to better than 10 cm/s. For this reason, the onboard filter only needs to update tile position; the velocity is assumed to be perfect and is not updated. Thus, corrections to the comet-centered position,  $\Delta \vec{X} = [\Delta x \ \Delta y \ \Delta z]^T$ , form the first three components of the estimate vector.

It was recognized fairly early that the knowledge of the spacecraft attitude was a major error source during encounter. During cruise, ACS determines the spacecraft attitude using a star tracker. During encounter, however, there is no guarantee that stars will be visible through the coma, so gyroscopes are used to obtain spacecraft attitude.

The gyros are initialized with values from the star tracker several hours prior to encounter, depending on the observed coma opacity. These initial values will have a bias associated with them. As time passes, the gyros will also drift, and have random perturbations which affect the measurements. The statistical nature of the biases and drifts can be determined beforehand, and are given in Table 1 [4].

The above values can be used to form a model of spacecraft attitude knowledge errors. A random sampling of

the values are taken and the gyro drift is computed as a function of time for each of the three spacecraft axes (Figure 4). The drifts are taken to be rotations about each of the spacecraft axes, that is, the true spacecraft attitude is a rotation about the computed spacecraft  $X$ ,  $Y$ , and  $Z$  axes with the magnitude given by the plots in Figure 4. The net effect on the observed positions is shown in Figure 5. The plots show what the data residual would look like if the trajectory knowledge and centerfinding ability were perfect, and the only error is caused by spacecraft attitude knowledge errors. It is clear that the effect on the data due to this error source is large and must be accounted for in the filter. Thus, in addition to corrections to the position, the filter estimates corrections to three components of spacecraft attitude: the right ascension ( $\lambda$ ) and declination ( $\delta$ ) of the body-fixed  $X$ -axis, and twist ( $\varphi$ ), the rotation about this axis.

### Filter Equations

The filter used to provide a state update at the current time,  $t_i$  is a standard extended Kalman filter. Due to the fact that the translational equations of motions are linear, and only corrections to the nominal attitude are needed, numerical integration is not needed which greatly simplifies the filter. First, the observation partial derivatives with respect to the state,  $H_i$ , is:

$$H = \frac{\partial(y, I)}{\partial(\Delta x, \Delta y, A_2, \Delta \lambda, \Delta \delta, \Delta \varphi)} \quad (20)$$

The partials are computed numerically using central differences. For example, the partial of pixel or line with respect to one of the estimated parameters,  $q$ , is:

$$\frac{\partial p}{\partial q} = \frac{p(q + \delta q) - p(q - \delta q)}{2\delta q} \quad (21)$$

where  $p, I = f(\vec{X}, \lambda, \delta, \varphi, \theta)$  and can be computed using Eqs. (1)-(10). To get the dependence on  $\lambda, \delta$ , and  $\varphi$ , note that  $T_{IBF}$  in Eq. (4) can be computed as

$$T_{IBF} = R_1(\varphi)R_2(-\delta)R_1(\lambda), \quad (22)$$

where  $R_1, R_2$ , and  $R_3$  are rotations about the spacecraft  $X, Y$ , and  $Z$  axes, respectively.

Since the only estimated parameters are the position and constant attitudes, the state transition matrix to map estimates from  $t_{i-1}$  to  $t_i$  is the identity matrix. Thus, the a-priori covariance at  $t_i$  is the same as for  $t_{i-1}$ , that is,

$$\bar{P}_i = \bar{P}_{i-1}. \quad (23)$$

The standard form of the Kalman gain matrix can then be written as:

$$K_i = \bar{P}_i H_i^T (H_i \bar{P}_i H_i^T + R_i)^{-1}. \quad (24)$$

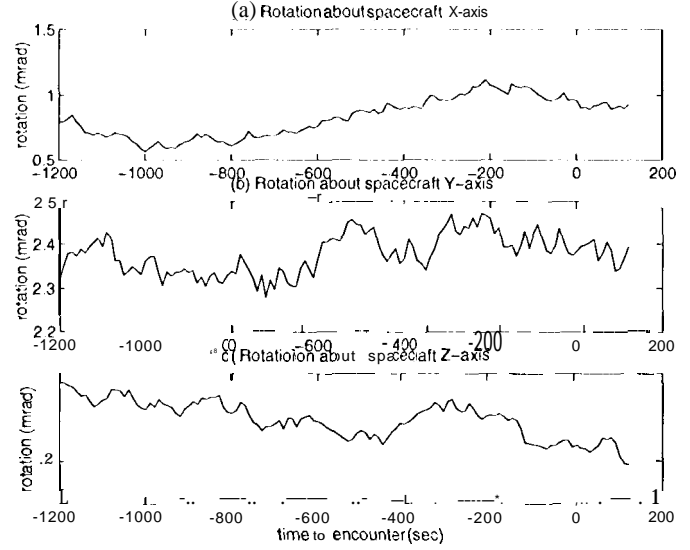


Figure 4: Gyro Drifts vs. Time for 3 Spacecraft Axes

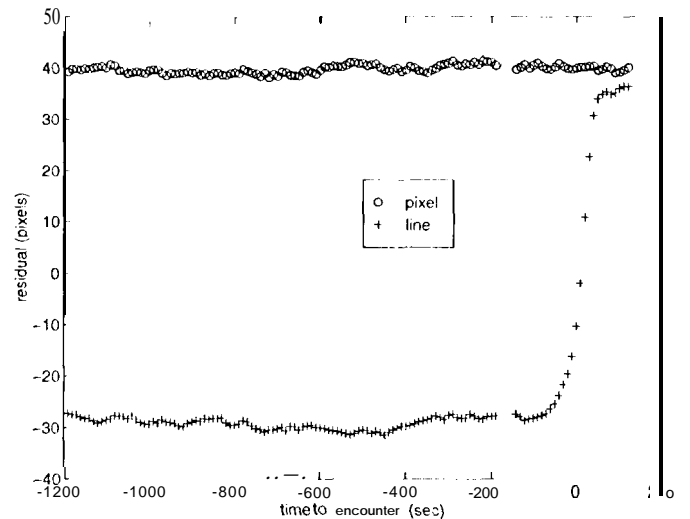


Figure 5: Pixel/Line Residuals Due to Spacecraft Attitude Knowledge Error

Here,  $R_i$  is a diagonal weighting matrix,

$$R_i = \begin{bmatrix} \sigma_p^2 & 0 \\ 0 & \sigma_l^2 \end{bmatrix}, \quad (25)$$

where  $\sigma_p^2$  and  $\sigma_l^2$  are the weights on pixel and line, respectively. The data weight is the square of the assumed radius of the nucleus in pixel space, which, assuming a 2 km nucleus radius, varies from minimum of 4 pixels at W-20 minutes to a maximum of about 220 pixels at encounter. The updated estimate of the state,  $\hat{x}$ , is then given by:

$$\hat{x} = \begin{bmatrix} \Delta x \\ \Delta y \\ \Delta z \\ \Delta \lambda \\ \Delta \delta \\ \Delta \varphi \end{bmatrix} = K_i \begin{bmatrix} p_o - p_c \\ l_o - l_c \end{bmatrix}, \quad (26)$$

where the observed centers,  $p_o$  and  $l_o$  are obtained from the centroiding process, and  $p_c$  and  $l_c$  are computed using Eqs. (1)-(10) and the nominal value for  $\bar{X}$ . Finally, the updated covariance at  $t_i$  is calculated as:

$$P_i = (I - K_i H_i) \bar{P}_i. \quad (27)$$

Given the equations for the Kalman filter, the centroiding process, and the inertial to camera transformations, the algorithm to do the updates can be described. Prior to starting the autonomous tracking, the software is initialized with the current camera model, predicted nucleus size, and the spacecraft state (position and velocity) as determined from ground-based navigation at the start time. The covariance on the initial position is also provided. As each image is taken by the camera (at a nominal frequency of one every 10 seconds), the tracking software is run to update pointing predicts for the next image. The inputs to the process as it is running are:

- The shutter open time for the current image.
- The 3x3 inertial to spacecraft body-fixed rotation matrix,  $T_{IBF}$ , at the time the image was shuttered.
- The mirror angle,  $\theta$ , at the time the image was shuttered.
- The image itself.

The algorithm used to generate a predict for the next picture opportunity when provided the above information with each picture is as follows.

1. Compute the current spacecraft right ascension, declination, and twist by decomposing the  $T_{IBF}$

matrix using the equations:

$$\begin{aligned} \lambda &= \tan^{-1} \left( \frac{T_{IBF}^{\prime}(1, 2)}{T_{IBF}^{\prime}(1, 1)} \right) & (28) \\ \delta &= \tan^{-1} \left( \frac{T_{IBF}^{\prime}(1, 3)}{A} \right) & (29) \\ \varphi &= \tan^{-1} \left( \frac{T_{IBF}^{\prime}(2, 3)}{T_{IBF}^{\prime}(3, 3)} \right) & (30) \end{aligned}$$

where

$$A = \sqrt{T_{IBF}^{\prime}(1, 1)^2 + T_{IBF}^{\prime}(1, 2)^2}. \quad (31)$$

2. Add the previously filtered attitude corrections,  $\Delta \lambda$ ,  $\Delta \delta$ , and  $\Delta \varphi$  to the ACS provided attitude in Eqs. (28) to (30). For the first image that is processed, these corrections are assumed to be zero.
3. Add previously filtered corrections to the nominal position and propagate the position to the current time. The corrections will be zero for the first image.
4. Process the picture to get the observed nucleus center location, using the nominal current position to start the search and to get the range to the nucleus to compute data weights.
5. Compute a corrected spacecraft attitude,  $T_{IBF}^{\prime}$  using the updated attitude from step (2), using Eq. (22).
6. Using the current position and corrected attitude, find new estimates for current position and corrections to the attitude with the filter equations shown in Eqs. (20) to (27). Only one iteration is needed for convergence.
7. Store the updated position and attitude corrections for use when the next image is obtained.

## 6 MONTE CARLO SIMULATION AND RESULTS

### Introduction

If the dynamic equations used in the filter precisely modeled the true forces acting on the spacecraft, then the covariance obtained after filtering would accurately represent the statistics of the estimated values. This is clearly not the case however, as we have deliberately used a reduced set of dynamics to keep the algorithm simple and fast. For this reason, Monte Carlo simulations are needed to assess the ability of the algorithm to maintain visual lock on the nucleus. For the simulations, a "truth" model of the trajectory, spacecraft attitude, and observations are generated and provided to the filter. For a given run,

the truth model represents a random sampling of the error sources which affect that model. One-hundred runs are performed, and the results are evaluated by determining whether or not the nucleus was visible in the camera FOV at all times. The details of this process will now be described.

### Trajectory Model

The truth trajectory is integrated forward from the starting conditions using numerical integration of the full translational equations of motion of the spacecraft. These equations include the central body force from the sun, plus third body perturbations from the nine planets and solar radiation pressure. The starting conditions are obtained from a random sampling of the position uncertainties at time of initiation for autonomous tracking, which is assumed to be 20 minutes prior to the nominal encounter time. From the latest ground-based navigation studies, it has been determined that the uncertainties in position at this time are 8 km in the cross-track direction and 150 km in the down-track (all 1a). For the simulation then, independent random samples of these values with a Gaussian distribution are drawn for each run, rotated into the comet-centered cartesian coordinate system, and added to the nominal initial state. The position and velocity are propagated using a Runge-Kutta 4th order integrator. Since the truth trajectory is known, it can be compared to the filtered position estimates to assess filter performance.

### Spacecraft Attitude Model

During actual flight, the spacecraft attitude will be maintained using a closed-loop ACS control system [5]. The closed-loop system is necessary because it is expected that particle impacts on the Whipple shield during flyby will cause attitude excursions which the control system must correct. Knowledge of the current attitude is provided by gyros which are initialized around 5 hours prior to encounter. The requirement is that the control system be able to recover from attitude hits of up to 2°. Excursions this large, however, will result in 10ss of the image because it takes time to return to the correct attitude. The frequency of this happening is unknown at present, and highly dependent on dust density models which are currently thought to be accurate only to an order of magnitude.

Simulations of the ACS control system are being performed at Lockheed Martin Astronautics; however full integration with the navigation autonomous tracking will not be accomplished until November of 1997. Thus, the spacecraft attitude model in our current simulation only incorporates the gyro drift model described in Table 1

above, which assumes errors in attitude knowledge but perfect control. Once again, Gaussian distributions of the initial bias and random noise are sampled for each of the three axes, and a time history of the rotations about the axes are generated (Figure 4). Starting with the nominal inertial to spacecraft body-fixed rotation matrix, incremental rotations from the error sample are applied at each image time and passed to the tracking algorithm to mimic ACS's attitude knowledge. The "truth" attitude in this case is simply the nominal, which can be compared to the filtered estimates from the algorithm.

### Observation Model

The ability to compute a nucleus centroid from the image is a crucial component of the tracking algorithm. In order to properly test this component, accurate representations of the comet nucleus and coma arc needed. This is a difficult task however, and still a work in progress, particularly since parameters which describe the coma brightness and dust densities have large uncertainties associated with them. Nevertheless, some simple simulated images have been generated and the centroiding algorithm does perform fairly well in determining their centers.

The use of generated images for Monte Carlo simulations is necessarily limited, though, due to the large amount of time needed to produce a single 1024 square image. Instead, the general characteristics of the observed centroids can be deduced from a single run through one sample encounter scenario and applied empirically for others. These general characteristics are a function of the size and rotation rate of the nucleus, and the phase angle at which it is observed. The procedure used to produce simulated observables is as follows. Here, primes represent "true" values for the various quantities.

- Compute the true center of the nucleus,  $p'_o, l'_o$ , in the camera FOV by finding the relative spacecraft to comet vector, using the integrated truth spacecraft trajectory, and then transforming to pixel/line coordinates using Eqs. (1)-(10).
- Compute simulated brightness offset by using Eq. (15) and (16) in reverse,

$$p'_{cb} = p'_o + \gamma(F'_s R'_c) \cos \phi + (\text{ff. 1t}) \&. \quad (32)$$

$$l'_{cb} = l'_o - \gamma(F'_s R'_c) \sin \phi + (F'_r R'_c) \sigma_r. \quad (33)$$

Here,  $F'_s$ , the multiplier to the true radius in Eqs. (32) and (33) is a scale factor to obtain brightness shifts as a percentage of the true radius. The parameter can be varied to simulate the effects of different shapes and its effects on the brightness centroid. The third term in (32) and (33) is used to add random noise the simulated brightness centroid, with a magnitude once again a percentage of the

true nucleus radius.  $\sigma_r$  is a random sample of Gaussian noise taken at each image with a mean of zero and unit standard deviation

## Results

The results of a 100 sample Monte Carlo simulation to test the nucleus tracking algorithm is shown in Figure 6. For these runs, the truth state was sampled from the nominal uncertainties of 8 km crosstrack and 150 km down-track and the truth attitude was sampled from the gyro error model in Table 1. The observations were obtained using values of  $F_s$  and  $F_r$  of 1.0 and 0.25, that is, the brightness shift was 100% and random noise 25% of the radius, respectively. The true target radius was set at 2.6 km, whereas the filter assumed a 2.0 km radius. Observations were taken starting at W-20 minutes to W+2 minutes, with a 40 second gap starting at W-180 seconds to account for the roll maneuver. Figure 6 plots the difference between the true spacecraft position and estimated position at each observation time in the down-track, out-of-plane crosstrack, and in-plane crosstrack directions, for all 100 samples.

Qualitatively, it is clear from the plots that the initial position error is being removed by the filter. Some simple quantitative checks can be made also. First, it can be noted that the out-of-plane crosstrack error must be roughly less than half the camera FOV ( $1.75^\circ$ ) at the time of the roll maneuver initiation so that the nucleus will sweep by in the correct mirror plane. Given a nominal flyby distance of 150 km, a  $3\sigma$  in-plane error places the minimum flyby at 125 km, so multiplying this value by the tangent of  $1.75^\circ$  gives about 3.7 km. Thus, if the out-of-plane error at roll initiation is greater than 3.7 km, most of the nucleus will be lost. The upper and lower 3.7 km boundary is marked as dashed lines in Figure 6(b), and it is seen that at W-180 seconds, the error in all 100 samples is less than this amount.

The down-track error behaves slightly differently. At a far distance, the down-track error has no effect on camera pointing since the camera boresight is effectively parallel to the down-track direction. As the comet approaches, the down-track error rapidly rotates into the camera focal plane until encounter is reached, at which time the maximum error that can be tolerated is the same as for the crosstrack, 3.7 km. The envelope described by the maximum error is shown by the parabolic dashed lines in Figure 6(a) (earlier than W-420 seconds, it is off the scale). Again, all 100 sample errors are below the threshold.

As a final check, a circle describing the projection of a spherical nucleus into the camera focal plane was computed at each image. If over 10% of this circle was out of the camera FOV, the image was flagged bad and it was

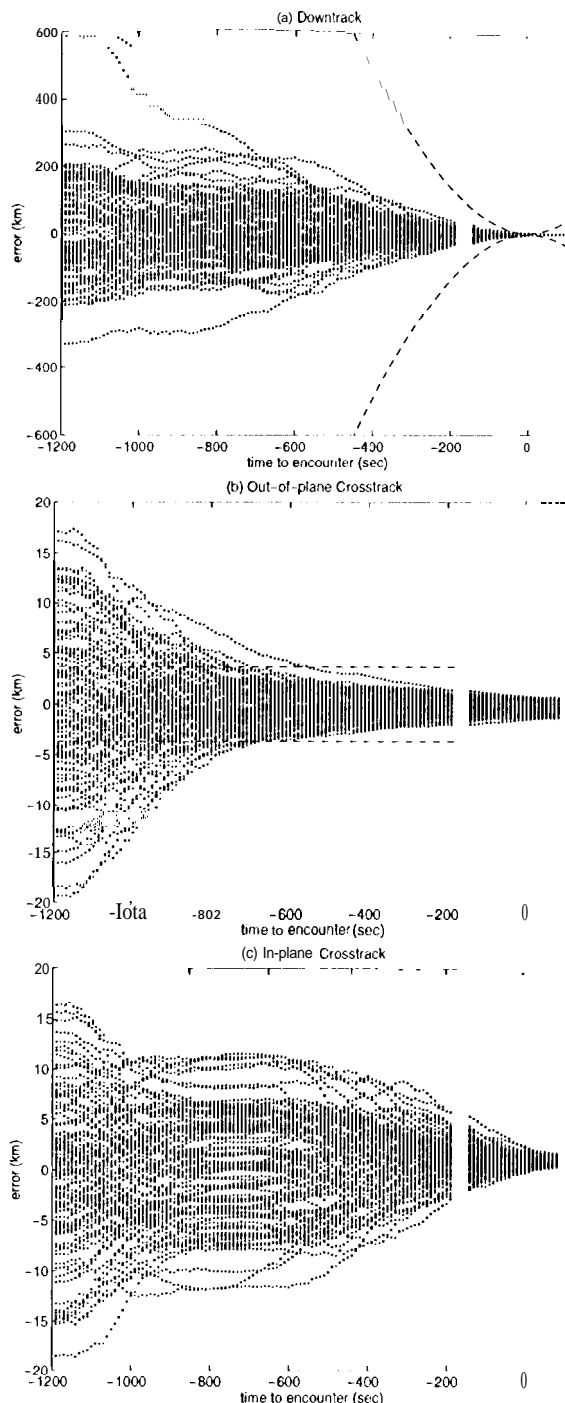


Figure 6: Position Errors (Estimated - Truth) for 100 Monte Carlo Simulations

assumed the nucleus was lost. Given the nominal values for the error sources, only two of the 100 samples run lost the nucleus according to this criterion.

This test assumed that all images were available and could be properly processed for centroid information. It is likely though, that images will be lost, either due to the spacecraft attitude being knocked off by particle impacts, noise in the images which throw off the centroiding, or other factors. Thus, a second simulation was performed where approximately 40% of the images were deleted, where the deleted images were distributed randomly through the run. The results showed that even in this case, the algorithm performed successfully, with only 3 out of 100 failures as determined by the circle criterion.

A third variation to test the system was to double the uncertainties on the gyro model given in Table 1. In this case, the amount of loss due to the circle criteria was 12 out of 100. However, the probability of getting at least some part of the nucleus is still fairly high. This can be seen graphically by examining the histogram plots in Figure 7 and Figure 8. These show the spread of the estimated errors in the out-of-plane cross track direction at the initiation of the roll maneuver (W-180 sec), and error spread of the downtrack direction at the nominal encounter time, for the nominal case in (a) and degraded attitude knowledge in (b). The vertical dashed lines show the threshold error at which the nucleus is more than half out of the camera FOV. In Figure 6(b), it can be seen that only one sample was greater than the threshold, indicating that the correct orbital plane was determined 99% of the time. In the downtrack direction, 4 or 5 samples were above the threshold which means that in these cases, the encounter images were lost. Thus, for about 94% cases, part of the nucleus was still in the FOV.

A final variation was to double the initial navigation position uncertainties. The results from this run are plotted in the histograms in Figure 7(c) and Figure 8(c). In this case, the roll maneuver was accurately determined for all cases, but the downtrack distance was missed in about 8 of them. This is reflected in the circle test., with 8 out of 100 losses. If, the ground-based navigation uncertainties are really this high, however, it is likely that the flyby distance will be increased, making it easier for the algorithm to correct the downtrack error.

## 7 TIMING

In addition to being accurate, a prime consideration in the algorithm development is the timing needed to perform all the tasks. The computer onboard STARDUST is a radial ion hardened R6000 processor capable of running at speeds of 5, 10, and 20 MHz (20 MHz will be used during encounter for the tracking code). This processor is similar to the PowerPC processor and uses much of the same

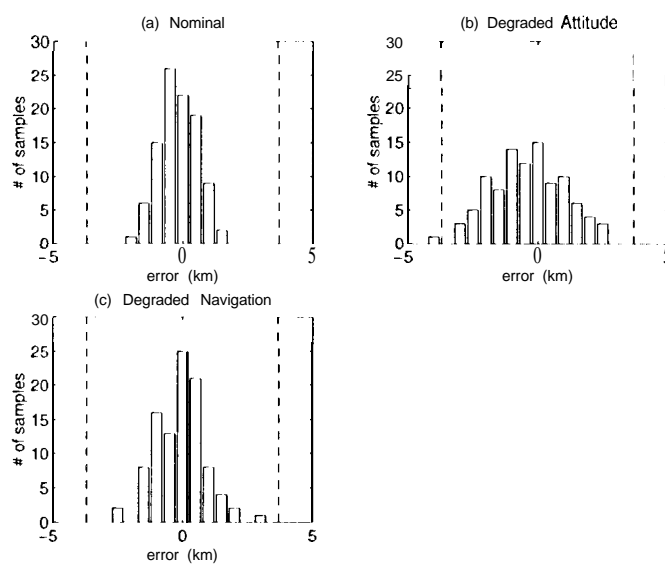


Figure 7: Histogram of Out-of-plane Crosstrack Errors (Estimated - Truth) at Roll Maneuver initiation Time

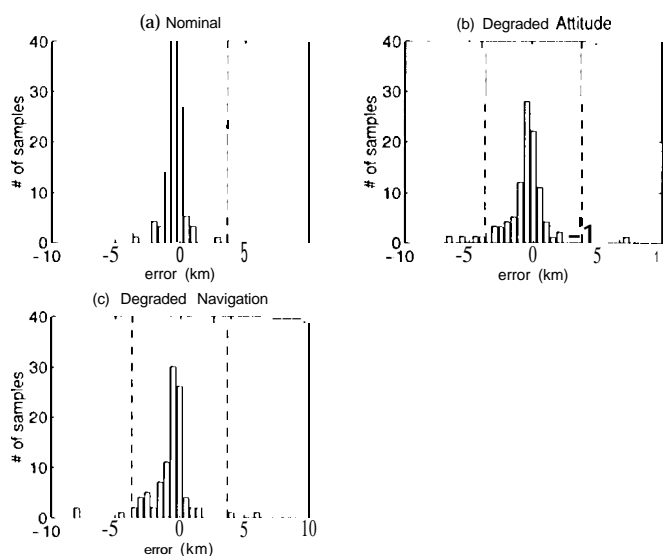


Figure 8: Histogram of Downtrack Errors (Estimated - Truth) at Encounter Time

architecture and code set. Timing tests have been done at Lockheed Martin on a PPC 603 running at 66 MHz to see how fast the algorithm performs. These tests show that the entire tracking code completes in approximately 2.7 seconds, with the majority of the time is taken up in the brightness centroiding portion [6]. Although the R6000 runs at a slower clock speed, it performs faster on floating point operations, so overall the timing degradation from PPC 603 to R6000 should not be very much. The 2.7 second time meets the requirement, but further speed-up is still being looked into. One simple way to do this is to centroid using every other, or every third pixel, in the brightness moment algorithm. This should not affect the centroid location at close distances when the nucleus will fill up a substantial portion of the camera frame, but will at far distances, so a range check would need to be made before subsampling.

## 8 CONCLUSIONS

The simulations described are a good first test of the algorithm to assess its performance. By themselves, however, they are not sufficient to completely prove its reliability. The two major areas where further work needs to be done are in comet visualization modeling and spacecraft attitude modeling. For the former, work is continuing on developing a realistic model of a comet, complete with irregularly shaped nuclei and a coma. These new images will then be provided to the centroider. Assuming different parameters for the dust density and other optical properties, the ability of the centroider to accurately find the nucleus can be tested under different conditions. If the simple brightness centroiding is not robust enough for the majority of cases, more complicated center finding algorithms need to be developed.

The spacecraft attitude modeling issue is important because it is yet uncertain how particle impacts will affect the tracking performance. This aspect was crudely simulated by randomly deleting some percentage of the images. During flight however, the losses will probably not be quite as random and may be concentrated in the minutes surrounding encounter when the dust density will be greatest. The onboard ACS will attempt to return the attitude to the correct orientation after impacts, but without coupling an attitude control simulation with the nucleus tracking algorithm, it is difficult to determine if the impacts will result in loss of tracking, and if so, at what level of impacts this happens. This test is currently scheduled to be performed sometime late in 1997.

Finally, it should be noted that, although the nucleus tracking algorithm was developed for the STARDUST mission, it can be easily applied to any mission that incorporates small body flyby. Current plans call for using a nearly identical version of the tracking code for the New Millennium Program's Deep Space 1 mission during its

flyby of an asteroid and comet [7]. Since both these flybys occur well before STARDUST reaches its target, they will provide a good realistic test of the system.

## ACKNOWLEDGMENT

The work described in this paper was carried out at the Jet Propulsion Laboratory, California Institute of Technology, under contract with the National Aeronautics and Space Administration.

## REFERENCES

- [1] W. M. Owen and R. M. Vaughan, "Optical Navigation Program Mathematical Models" JPL Internal Document JPL-EM 314-513, August 9, 1991.
- [2] J. Riedel, W. Owen, J. Stuve, S. Synnott, and R. Vaughan, "Optical Navigation During the Voyager Neptune Encounter" AIAA/AAS Astrodynamics Specialist Conference, AIAA-90-2877, Portland Oregon, August, 1990.
- [3] S. P. Synnott, A. J. Donegan, J. E. Riedel, J. A. Stuve, "Interplanetary Optical Navigation: Voyager Uranus Encounter", AIAA Conference, Williamsburg, Virginia, August, 1986.
- [4] E. P. Lander, Lockheed Martin Astronautics, Denver, CO, personal communication.
- [5] E. D. Lander and S. E. Hollar, "Attitude Control and Survival of the STARDUST Spacecraft During the Coma Passage of Wild-2", AAS 97-005, AAS Guidance and Control Conference, Breckenridge, CO, February, 1997.
- [6] D. Gingerich, Lockheed Martin Astronautics, Denver, CO, personal communication.
- [7] J. E. Riedel, S. Bhaskaran, S. P. Synnott, S. D. Desai, W. E. Bollman, P. J. Dumont, C. A. Halsell, D. Han, B. M. Kennedy, G. W. Null, W. M. Owen, R. A. Werner, and B. G. Williams, "Navigation for the New Millennium: Autonomous Navigation for Deep-Space-1", Proceedings 12th International Symposium on Flight Dynamics, Darmstadt, Germany, June, 1997.

**Shyam Bhaskaran** is a Senior Engineering Staff member of the Optical Navigation Group at the Jet Propulsion Laboratory. His current tasks include the design, development, and testing of the autonomous navigation system for the New Millennium Deep Space 1 mission. In addition, he is also responsible for developing and testing the autonomous nucleus tracking system for the STARDUST mission. In the past six years at JPL, he was also a navigation team member of the Galileo mission, and has participated in several advanced studies for radio and optical navigation systems for future missions. Dr. Bhaskaran received his B. S. and M. S. at the University of Texas at Austin, and a Ph. D. at the University of Colorado in Boulder, all in Aerospace Engineering.

**Joseph E. Riedel** received a B.S. in physics and astrophysics from the University of California, Irvine in 1978. Immediately joining the Voyager Navigation Team at JPL, he participated in all planetary encounters of both spacecraft, and was the lead optical navigation engineer for the Neptune flyby. After leading the opnav efforts for the Galileo asteroid flybys and early Galilean tour, he became the New Millennium Navigation Team chief, directing the development of a completely autonomous optical navigation system to guide the approach and flyby of DSI past an asteroid, Mars and a comet. He is an author of numerous papers on navigation, optical navigation and navigation-related image processing technology.

**Stephen Symnott** received a PhD degree from the Aeronautics and Astronautics department at MIT in 1974 and has been in the Navigation Section at JPL ever since. He is currently supervisor of the optical navigation group in that section. He was leader of optical navigation operations for both the Voyager and Galileo missions, and has been involved in many studies of future planetary missions and the use of radio tracking data for navigation and planetary science purposes. Most recently he has supervised the development of an autonomous optical navigation system for interplanetary missions to be flown for the first time on the New Millennium Deep Space 1 mission. Dr. Symnott has discovered 13 previously unknown satellites of the outer planets using Voyager imaging data. He is a member of the American Astronomical Society and the International Astronomical Union.